Petroleum and Coal

Article **Open Access**

Enhanced Reservoir Characterization Using Petrographic Image Analysis

Chahenaze Mostafa Ellamey[1], *Attia Mahmoud Attia*[2]

[1] *Schlumberger Petroleum Company, Egypt*
[2] *Faculty of Energy and Environmental Engineering, British University in Egypt (BUE), Elshorouk City, Cairo, Egypt*

Received November 7, 2021; Accepted March 17, 2022

Abstract

Petrographic Image Analysis (PIA) is a new technique that provides valuable petroleum engineering data using both geological thin-sections and image analysis. PIA measures the geometry of 2D images, including pore geometry, to predict petrophysical properties, providing a time and cost-effective approach that does not require core plugs. The current research utilizes PIA and the freely available "ImageJ" image processing program to perform petrophysical, petrographical, and mineralogical reservoir rocks' characterizations, including porosity and permeability calculations, rock texture, porosity types, and diagenesis process descriptions, as well as lithology identification, respectively. Further, PIA results are compared with conventional experimental approaches' results for every sample's validation. The conventional laboratory approaches used for validation are Core visual observations for lithology and compaction observations, Core plug experiments and methods, including porosity saturation method, helium porosimetry method, liquid permeameter method, and Winland R35 rock typing method, for porosity, rock density, permeability, and rock typing purposes, and finally the X-ray diffraction analysis (XRD) for the rock mineralogical composition determination. To perform the current study, 40 core plugs of different lithologies, including sandstones, limestones, and dolostones, are obtained from El-Shoruk City in Egypt. Also, 40 2D blue-dye resin stained thin-section images, which match the 40 core plugs, are acquired for studying. Moreover, the current research aims to calculate permeability using three conceptually distinct and modified permeability equations that function in image geometry parameters. Furthermore, correlations between porosity values and permeability values, obtained from both graphical and experimental methods, are to be established for each lithology by use of correlating factors. Results show good accuracy of porosities and permeabilities obtained from PIA, logical description of petrography, and correct mineralogy identification for different lithologies.

Keywords: *Petrographic Image Analysis (PIA); permeability; rock typing; reservoir characterization; XRD for rock.*

1. Introduction

Rock properties including porosity and permeability are necessary for the development processes of any oil field. The development process is carried out using different techniques, such as chemicals, thermal and nanotechnology and other techniques [1-2].

Petrography is a branch of Petrology that focuses on minerals and textures of rocks, relates them, and allows rock description and classification [3]. Petrographic image analysis (PIA) and 2D thin sections allow the microstructure study of reservoir rocks, showing grains and pore spaces, by examination of a slice of the cross-section of the rock of interest held in between 2 glass slides under the microscope [4]. PIA is a technique used to measure the geometry of 2D images by use of statistics to predict petrophysical properties in case no information about the samples is available or the samples are small for core plug experiments, with the additional privilege of direct observation of pore structure, unlike core plug measurement. Many scientists and researchers have provided 2D and 3D numerical simulation methods to mimic the reservoir behavior and obtain correct petrophysical values from thin sections and images.

However, although 3D is closer to the real situation of the reservoir, still 2D simulation is less expensive, simpler, and more time saving and includes larger areas [5]. As permeability is essential in reservoir characterization, and laboratory work is costly and time-wasting, and core plugs are not always available, image analysis of 2D thin sections are highly used for pore structure description, and numerical methods and models are implemented and constructed, respectively for simulation of fluid flow and thus permeability estimations [6]. Also, additional useful data can be obtained from thin section analysis as mercury injection only works on the volume of pores of a certain neck size [7]. Moreover, computer image analysis methods are used to measure pore and grain parameters to derive several parameters for petrophysical properties' predictions, by working on the scanning electron microscope-back scattered electron image (SEM-BEI) and using the Kozeny Carman equation, under the assumption of pores with smooth walls and pore hydraulic diameter for permeability computation [8], which is stated as follow:

$$K_{CK}=\frac{\emptyset^3}{Kc\ So^2(1-\emptyset)^2} \quad (1)$$

where So = 4/п (pore perimeter)/(pore area)

Besides, combining the hydraulic radius of Poisseuille law for non-circular cross-sections of tube bundles into the Kozeny Carman equation, considering pores with a single hydraulic radius, gives the Kozeny Carman equation and the Hydraulic radius approximation, with results showing better permeability values than other approximate expressions as compared with laboratory permeabilities, but with overestimated values, when applying the equation [9]:

$$K=\frac{\emptyset*A^2}{6*P^2} \quad (2)$$

Moreover, Kirkpatrick equation and effective medium approximation conductance (EMA) considers isotropic cubic lattice network with conducting medium and bonds for fluid flow so that each bond has a certain conductance value, and then a single effective conductance Ceff needs to be calculated to represent the whole network. The concept is applicable for narrow and broad distributions, with Ceff tending to geometric mean conductance Cg for narrow distributions. Permeability is to be estimated as follow [9-10]:

$$K=\frac{(\frac{N}{1.47})\mathrm{Ceff}}{\mathrm{X}*\mathrm{At}} \quad (3)$$

where X is equal to 2 for sandstones.

Also, the flow conductance for any cylindrical pore based on the hydraulic radius concept is calculated as follow:

$$\mathrm{C\,C} = (\frac{\mathrm{A}^3}{2\mathrm{P}^2} - \left(0.3 * \frac{\mathrm{A}^3}{2\mathrm{P}^2}\right)) * 0.375 \quad (4)$$

Also, the previous concept, in combination with Darcy's law and by use of the "Image J" software, is applied on Scanning Electron Microscope (SEM) images for sedimentary rocks, using perimeters, areas, hydraulic radius, the conductance of each pore, correction factors, the number density of pores, and the effective pore conductance, and yields better permeability results than the Kozeny method [10-11]. Another research provides an image analysis software, developed at home, to determine petrophysical properties from drill cuttings of "multi-fractured horizontal wells". Work is performed on siltstone reservoir, using SEM and other microscopes ' images, to calculate rock porosity, composition, and texture. Results showed higher porosity values and more accurate cement quantification than those of previous conventional methods, with the observation that more cement is found in larger Quartz grains samples [12]. Also, a 3D scan method for estimating permeability from 2D images is presented and the permeability is obtained by the lattice-Boltzmann algorithm using the "pixel-based indicator simulation". Results do not match the true laboratory measurements, but a trend is observed when plotting the obtained permeability (normalized by the grain size squared) versus porosity for sandstone cores [13]. In addition, a developed method for 3D pores connectivity or permeability determination from 2D thin section images is the Euler-Poincare characteristic (EPC). It is an integrative topological measure that connects pores from 2D slice to another, providing 3D visualization of porous media, in terms of Betti numbers (0 and 1) [14].

Moreover, 3D micro-CT images along with machine deep learning (DL), specifically pore network modelling, provide quick and correct permeability estimation of complex carbonate rock. Porosity, formation factor, and 3D images are taken from thousands of 3D micro-CT images as inputs for DL models to calculate permeability. Results show that permeability values are consistent with those of direct simulation; however, with 3 times saved time [15]. Moreover, Winland R35 Method is used for effective pore throat radius calculation and classification by use of the general equation for Petrophysical Rock Type (PRT) that is presented as follow [16]:

$$\text{Log}(R_{35}) = 0.732 + 0.588 \log(k) - 0.864 \log(\varphi) \quad (5)$$

The rock type classes are divided as follows for ranges of pore throat sizes in microns: Mega for >10, Macro for 2 to 10, Meso for 0.5 to 2, Micro for 0.1 to 0.5, and Nano for <0.1 [17]. Moreover, A new method is developed for more accurate use of the Winland technique, relocating the "iso pore throat lines". Results are verified by comparison with static models, and this method has been computerized so that inputs of porosity and permeability are enough to compute R35, plot the graph, and provide slope ranges and rock types' numbers [18]. Sandstone samples are studied by the use of petrography and X-ray diffraction. Recently established a new technique for rock typing based on the resistivity data from logs [19]. The diagenesis process leads to compaction, change, and precipitation of grain structure, affecting porosity and permeability, as well as pore throat passages. Results show that samples are made mainly of quartz, that clay is more abundant in fine-sized sandstones, and that compaction occurred as indicated by grain contacts and dead-end pores [20]. Moreover, 2D and 3D Seismic, cores, cuttings, thin sections, well data and geology, and SEM photos are used to study the porosity and permeability of Limestone Breccia that accumulated in profound water. Noting that, the following porosity types were observed: Mouldic, Vuggy, intra-particle, inter-particle, inter-crystal, micro and macro, and stylolitic [21]. Another petrographic and mineralogical study is performed on a carbonate reservoir using cores and thin sections to describe rock properties and the lithology, reflecting the rock origin and environment of deposition. Results of SEM photographs and microstructure images of high resolution indicated that laminations of varve, silt, or mud sizes as well as big structures are found in carbonates of fine grains, with terrigenous, biogenic, and diagenetic materials among the grains [22]. Furthermore, researchers studied the impact of sorting and compaction on porosity distribution of sandstone cores, used X-ray computed tomography to acquire CT scans, and found that results comply with capillary pressure measurements [23-24]. Another X-ray CT scan study worked on studying the impact of grain size arrangement and consolidation pressure on porosity distribution of different properties rock cores. A density standardization correlating the CT number to bulk density to the porosity was performed. Also, a computer system was prepared to compute millions of porosity values for each core. Results were compared and proved effective CT scan capability in describing porosity changes [24]. Also, 2 high resolution imaging methods are developed to quantify each material connectivity on the microscopic scale, based on the concept of separation distance and travel time, respectively. Results of work performed on 1500 images of different connectivity, calculated upon organic components of shale samples captured in SEM images, proved accurate as compared with each other and with visual observation [25]. Another study focuses on obtaining 2D and 3D porosities and pore size distribution of Shale samples using image processing software and SEM images. A comparison between sandstone and shale samples is implemented to distinguish their pore characteristics. Results show that Shale connected porosity and pore size distribution are less than those of sandstone. Also, shale connected porosity was found inversely proportional to the sample size, while total porosity was found directly proportional to the size [26].

2. Experimental procedures

2.1. Core plugs and thin sections preparations

The experimental procedures are to be applied on 40 core plug samples and their corresponding 40 blue-dye resin stained thin section images of different lithologies. The 40 samples

are categorized as follows: 9 compacted calcareous sandstone samples, 12 compacted dolostone samples and 6 highly porous dolostone samples, and 13 nummulitic limestone samples, and are obtained from El-Shoruk area. Core plugs are cut and prepared from irregular reservoir rocks in specified lengths, diameters, and surface finishes to be used in special core analysis tests as they provide vital information of the investigated reservoir. Noting that, the ideal length of the core plug is from 75 to 80 mm to ensure accurate measurements and fit into laboratory devices. On the other hand, thin sections are made of prepared, smoothened, and pore stained rock chips of mainly 0.03 mm thickness [27]. Thin sections are pore stained for easier study and clearer view while examination under the petrographic microscope. As the rock chips are cut in small sizes, they can be easily obtained from rock cuttings without the need of core plugs, and are used for qualitative and quantitative analyses of the rock microstructure. Noting that, it is better to extract the core plug and the rock chip from the center of the reservoir rock to be a good representative of the available reservoir.

2.2. Conventional laboratory procedures

As the focus of this paper is on Petrographic Image Analysis, conventional laboratory measurements are only used as a reference to validate the PIA results. Regarding the petrophysical reservoir characterization, porosity values are obtained from the porosity saturation method and the helium porosimetry method. the porosity saturation method involves the weight measurement of each fully water-saturated core, as well as the calculation of bulk volumes, pore volumes, and so effective porosities, while the helium porosimetry method measures porosities by pressurizing helium gas into each core, taking into consideration the sample dry weight, length, diameter, bulk volume, matrix cup size, blank numbers, fill pressure, and equilibrium pressure, applying Boyle's law, and solving by substitution in an excel sheet. Noting that, porosities obtained from helium porosimetry method are more accurate than those obtained from the porosity saturation method because helium has the privileges of inert and very small molecules, which can enter smaller pores without any side reaction. Moreover, permeability values are obtained from the liquid permeameter method. The liquid permeameter method involves the placement of each fully water-saturated core into the core holder, the application of 450-500 psi confining pressure for core isolation, the use of a pressure control unit for water flow out of the core, the measurement of a certain water volume output in a graduated cylinder, the record of the time by a stopwatch, the reading of the differential pressure, and finally the substitution into Darcy equation. Also, regarding the mineralogical reservoir characterization, lithology is obtained from porosity methods by dividing the core plug's dry weight by the grain volume and comparing the result with reference densities of sandstone, limestone, and dolomite. Also, mineralogical observations are obtained from core visual observations as follows: sandstone core visual observations show sand particles intercalated in the cores, while carbonate core visual observations show no sand particles intercalated in the cores. Besides, petrographic observations are obtained from core visual observations too as follows: Very smooth rock texture indicates compacted samples, medium rough rock texture indicates medium porous samples, and rough rock texture indicates highly porous samples.

2.3. Petrographic image analysis procedures

The petrographic optical microscope, with the privilege of stage rotation and changeable optical orientation, is used in the geology laboratory to obtain various microphotographs of the blue resin stained thin section samples under study. Those microphotographs include the pore and grain or crystal arrangements at the micro scale, enabling not only the description of rock mineralogy and rock texture, but also further petrophysical calculations using PIA. Then, porosity values and pore parameters are obtained from the analysis of blue-dye resin stained thin section images using the "ImageJ" program, which is a freely available image processing software that is used to distinguish pore areas from grain areas based on manual thresholding and highlighting of pore space, and so it calculates thin section image parameters including 2D porosity (% pore area), total thin section area, total pore area, total pore counts,

average pore perimeter and thus total pore perimeter (average pore perimeter multiplied by the total pore counts), and average pore area. Noting that, "ImageJ" generates an excel sheet of data.

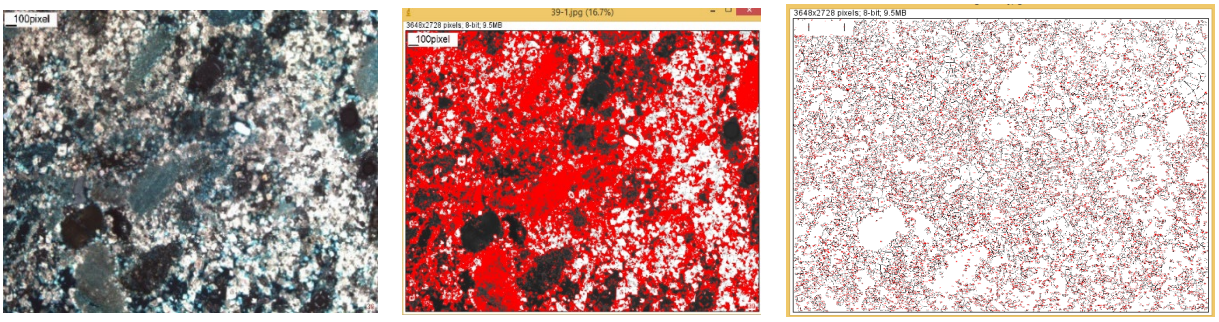

(a) (b) (c)

Slice	Total Pore Counts	Total Pore Area	Average Pore Area	% Pore Area	Average Pore Perimeter	Total Pore Perimeter
39.jpg	10223	4482499	438.472	45.042	84.227	861052.621

(d)

Fig.1, Image pore space manual thresholding and conversion into particle steps of High Porosity Dolostone using ImageJ software [28]. a) Original blue-dye resin stained thin section image. b) Thin section image after manual highlighting of pore spaces. c) Thin section image after pore space conversion into counts. d) Generated Excel Sheet by Image J

Also, permeability values are to be obtained using three permeability approaches that function in PIA pore parameters. Noting that, the permeability approaches are modified, then applied. Also, the scale of the images analyzed is in micrometer; therefore, the permeabilities obtained must be multiplied by 1.013171226 to be converted from um^2 into Darcy. Moreover, regarding the petrographical reservoir characterization, by comparison between thin-section images of samples and those of previously captured, studied, and classified samples of different lithologies of books and papers cited in the introduction, the description of the origin of rock deposition, possible post-depositional changes, porosity types, pore-grain structure, and pore connectivities by direct observations are applied. Furthermore, the observation of the grains' forms, types, and colors is applied to detect the mineral composition and so the determination of the lithology is based on the most occupying mineral and grains observed. For example, quartz grains show a grey color, dolomite crystals show a white color of rhombi crystals, calcite crystals show grey to brown color (calcite mud), and nummulitic limestones show the form of grey nummulites.

2.4. X-ray diffraction analysis (XRD)

Moreover, a part of the core plug which corresponds to the same thin section is cut and crushed into a powder for X-ray diffraction analysis, which is used as a reference to provide a mineralogical composition, and so validate the lithology identification from thin sections. As, XRD focuses X-ray beams on the powder of the rock understudy and gives the mineral compositions showing both the major and minor minerals present, by generating plots of mineral heights versus position. Noting that, high peaks of mineral heights indicate the major, most occupying, minerals, while low peaks of mineral heights indicate minor minerals [29].

2.5. Winland R35 rock typing method

The Winland R35 rock typing method is used as a way to compare petrographic results with laboratory results, as R35 is functioning in porosity and permeability, which are obtained once

in the laboratory and once using PIA. The comparison is based on the samples' classifications based on the ranges of pore throat sizes (um): mega, macro, meso, micro, and nano.

3. Results

It is to be noted that, in the following analysis, the 40 2D blue-dye resin stained thin section images, corresponding to 40 core plugs and 9 thin section slides of multiple lithologies, obtained from El-Shoruk area, are split into 3 sections based on the lithologies and obvious rock types and then combined as total samples in the 4th section. Moreover, the correlations and coefficients of determination R^2 are written on the plots: R^2 must be > 0.8 for accurate results.

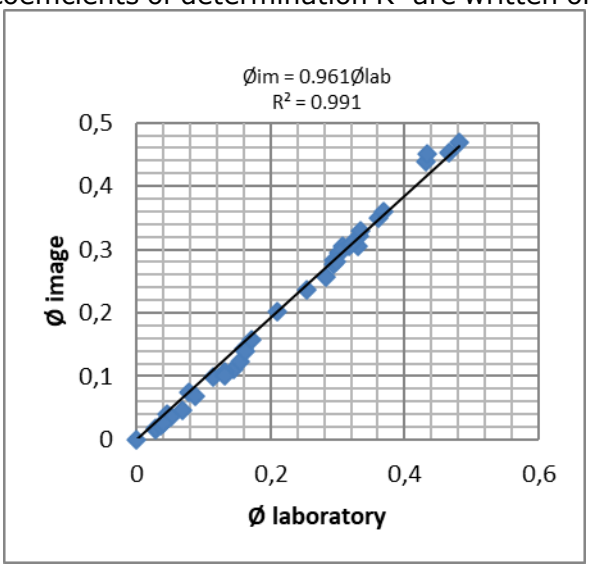

Fig.2. All samples image porosity vs laboratory porosity

Also, in the K image versus K laboratory and in the K image versus Ø image plots, the green color stands for Kozeny Carman equation, the blue color stands for Kozeny Carman equation and hydraulic radius approximation, and the red color stands for Kirkpatrick equation and effective medium approximation conductance, but first, verifications of image porosities of all samples for further application in permeability equations are needed. As indicated in Figure 2, the Ø image versus Ø laboratory plot yields an accuracy of the coefficient of determination R^2> 0.9, indicating accurate porosity estimation by image analysis.

Moreover, in addition to the porosity and permeability plots and R^2 values, average ratios of laboratory permeability to image permeability for all the thin section images, along with their variances σ^2 are used to assure the best permeability equation for each thin section, which must have a low variance, by use of the equation:

$$\sigma^2 = \frac{\sum\left(\frac{\text{k laboratory}}{\text{K image}} - \frac{\text{K laboratory of each sample}}{\text{K image of each sample}}\right)^2}{\text{number of samples}} \quad (6)$$

and lastly calculate average ratio factors that are specific for each lithology, by averaging the average ratio factors of thin sections of the same lithologies. Noting that in table 1, the best permeability equation for each lithology is stated and selected after average ratios factors and variances for the other permeability equations have been calculated, compared, and excluded as they give higher variances**.**

Table 1. All samples permeability laboratory/permeability image ratio factors and variances

Lithology	Equation	Average of Klaboratory/Kimage ratio factor	Variance (σ^2)
Compacted calcareous sandstones	Kirkpatrick equation and effective medium approximation conductance	0.956	0.009
Compacted and highly porous fossiliferous dolostones	Kozeny Carman equation and hydraulic radius approximation	0.186	0.004
Medium porous nummulitic limestone	Kozeny Carman equation and hydraulic radius approximation	0.182	0.003

3.1. Compacted calcareous sandstone samples

3.1.1. Petrophysical reservoir characterization using PIA

It is to be noted that, image permeability values are related to laboratory permeability values as indicated in Figure 3 (a); however, although that they do no give the same values, image permeabilities are multiples of laboratory permeabilities, so they need modification by

multiplying by a fixed fraction for each equation. Figure 3 (b) shows the K image modified vs K laboratory plot, which is after the permeability modification and that indicates that the best permeability equation to be used in compacted calcareous sandstones is the Kirkpatrick equation and effective medium approximation conductance with highest R^2 = 0.935, with corresponding multiplying fraction and lowest variance (σ^2), as shown in Table 1. However, although the R^2 of K image versus Ø image plot of this equation is not the highest in Figure 3 (c), still it is greater than 0.8, which makes it valid for this lithology as supported by the other 2 previous references: the R^2 of K image modified vs K laboratory plot and the lowest variance of the multiplying constant for the same equation.

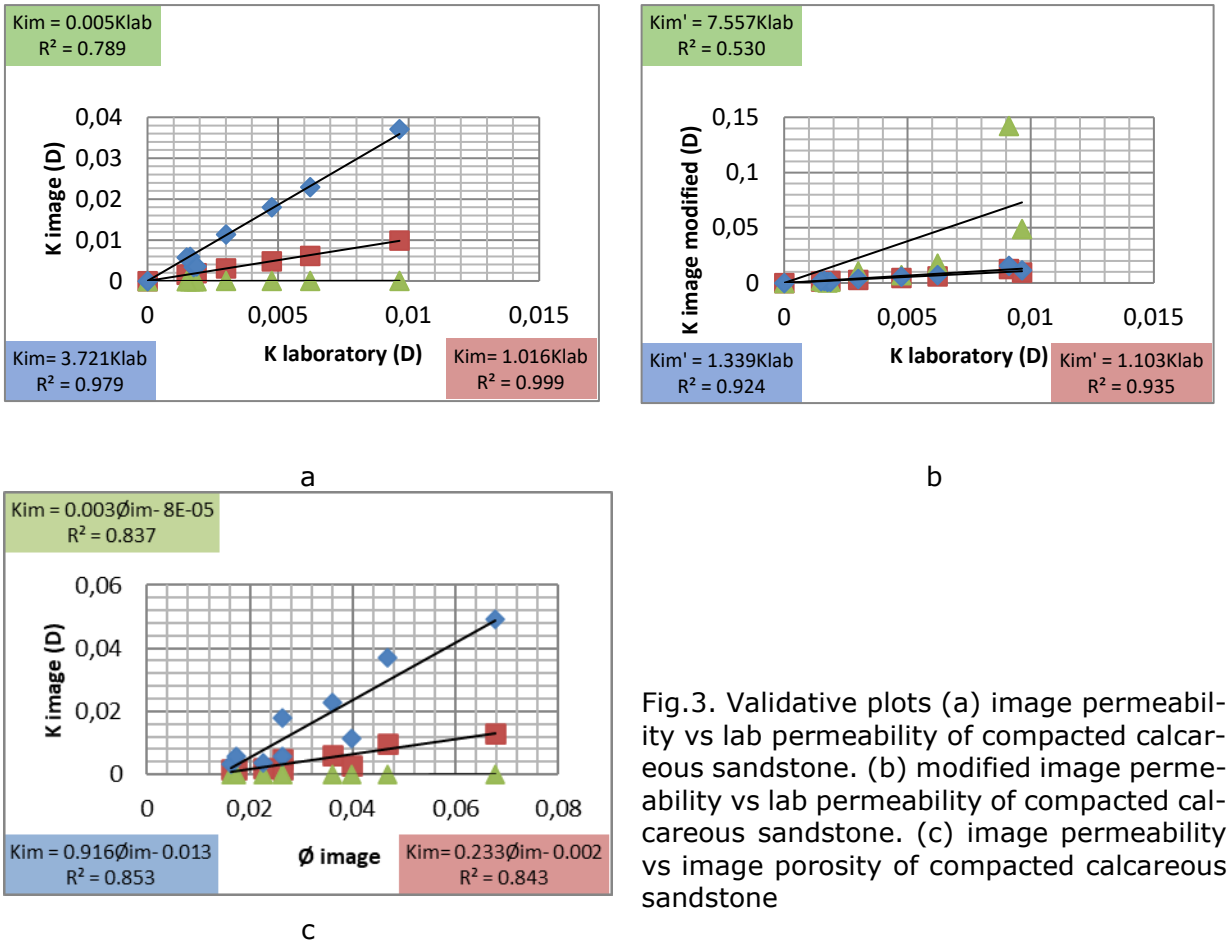

Fig.3. Validative plots (a) image permeability vs lab permeability of compacted calcareous sandstone. (b) modified image permeability vs lab permeability of compacted calcareous sandstone. (c) image permeability vs image porosity of compacted calcareous sandstone

3.1.2. Petrographical and mineralogical reservoir characterization using PIA

3.1.2.1. Petrographical reservoir characterization

Figure 4 shows the compacted micro-crystalline non-clastic texture of limestone crystals as well as the clastic texture of quartz grains. Noting that, the rocks are impregnated with blue dye-resin to display porosity and that the pore space is made up of isolated minor pores, resulting from the dissolution of calcite crystals (acting as cement), indicating marine environment was once existing with water dissolutions and intraparticle porosity, surrounded by many poor sorted (largest particles bigger than 10 times the smallest ones, diameter-wise) and compacted quartz grains (tightly packed grains, precipitated in the same environment, with low bulk volume and pore space, indicating deep high-pressure formation, and calcite cement show the close connection of grains, affirmed by point, line, concave, and convex grain contacts) of different shapes and sizes, with most dominant border shape: Angular so-called Breccias (considered as mineral grains instead of rock fragments) and most dominant size: Gravel (from 4mm to > 256 mm in diameter). Sand particles' roundness involves angular and

subangular borders, and sand particles' Sphericity indicates quartz chips produced by crushing [30]. The pores are mainly non-effective, isolated pores, with no connectivity, indicating very low permeability.

3.1.2.2 Mineralogical reservoir characterization

Lithology by thin section images observation

Figure 4 shows that the compacted calcareous sandstone samples are made up mainly of quartz grains (grey color) cemented by calcite mud background: calcite crystals (grey-brown color).

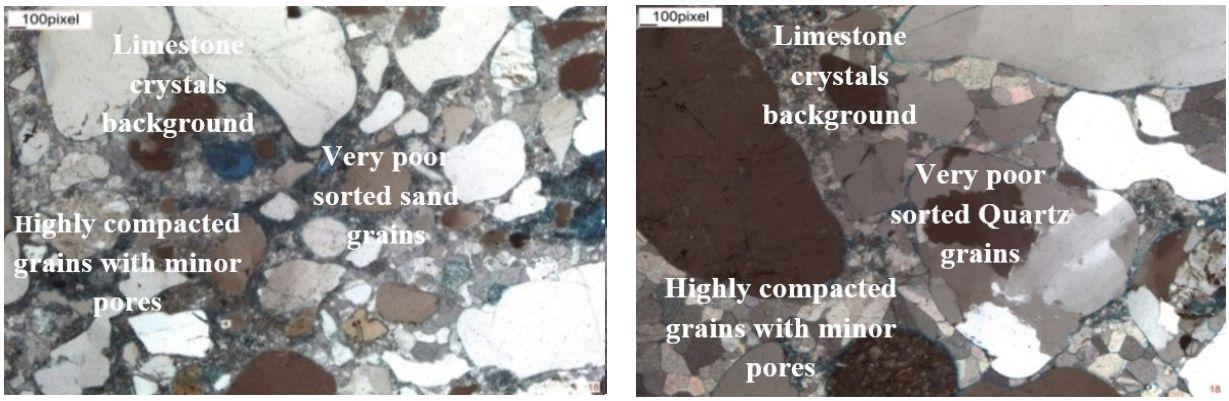

(a) **(b)**

Fig. 4. Microphotographs of compacted calcareous sandstones. (a) and (b) represent 2 of the 9 microphotographs for this lithology.

Other lithology references:

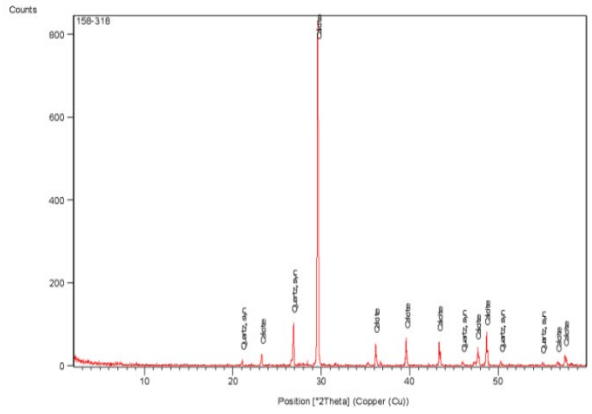

Fig. 5. Compacted calcareous sandstone xrd analysis mineral heights vs position

a) XRD analysis

As shown in figure 5, XRD analysis of Compacted Calcareous Sandstone shows that calcite has the highest XRD peak and so intensity, indicating limestone lithology and mineral composition of 74% Calcite (CaCO3), and 26% Quartz (SiO2).

b) Core visual observations

Compacted Calcareous Sandstone Samples show Sandstone core visual observations: Greyish white and medium rough rock texture, with sand particles intercalated in the cores.

c) Core plug densities

Compacted Calcareous Sandstone Samples show Sandstone core plug densities

Lithology result

Thin Section Images observations, regarding the lithology, comply with core visual observations and core plug densities. However, XRD analysis indicates Sandy Limestone instead, as it presents more calcite mineralogical percentage contribution than quartz, which is not the case as indicated by the other methods and which can be explained as follow: XRD measures based on x-ray beam spot on the powder of the sample, so if the powder taken for analysis is not representative of the entire sample (poor sampling), wrong results will occur, especially if the powder is taken from a single part of the sample, pointing to the importance of using multiple methods for lithology validation.

3.2. Compacted and highly porous dolostone samples

3.2.1. Petrophysical reservoir characterization

After applying the permeability modification as performed in the preceding samples, figure 6 (a-b) indicate that the best permeability equation to be used in compacted and highly porous fossiliferous dolostones is the Kozeny Carman equation and hydraulic radius approximation with highest R^2 = 0.937 and 0.825, respectively, of K image modified Vs K laboratory plots, with corresponding multiplying fraction and lowest variance (σ^2), as shown in table 1, and R^2= 0.941 of K image versus Ø image plot.

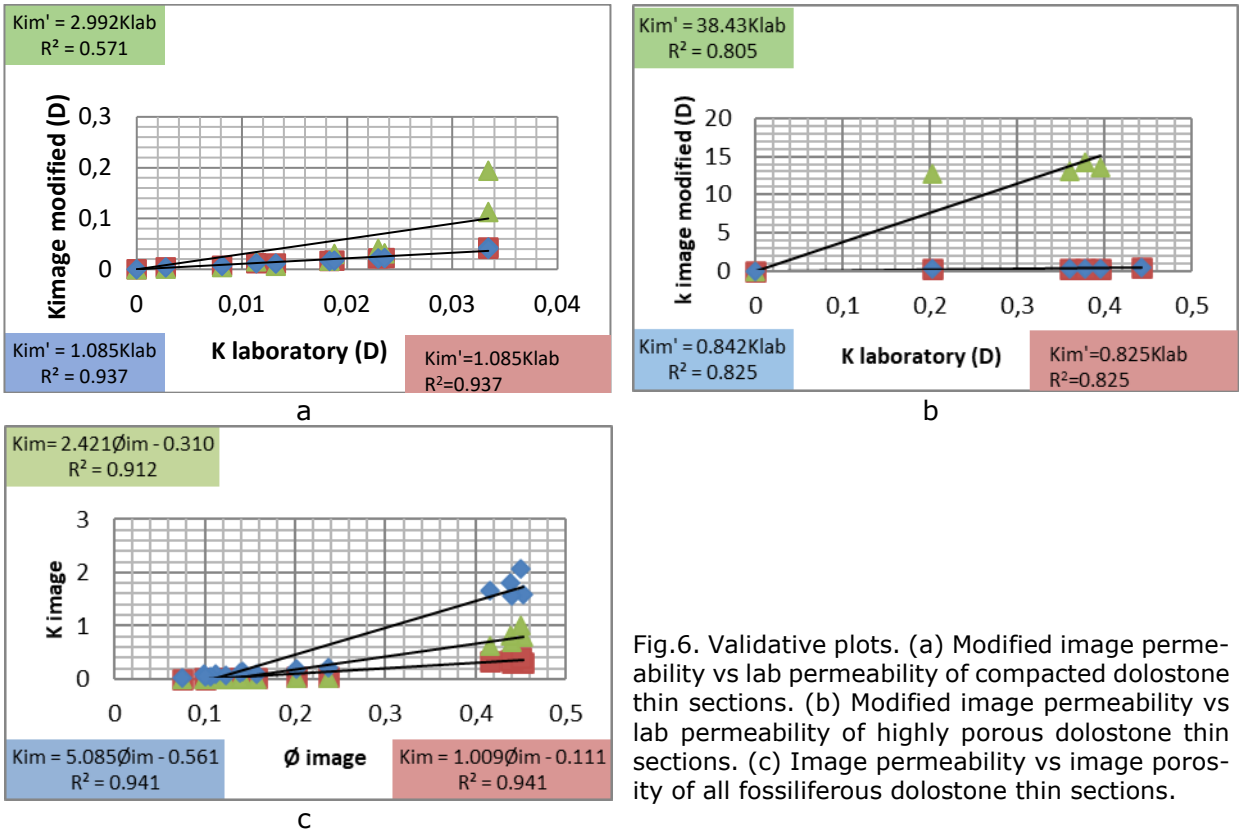

Fig.6. Validative plots. (a) Modified image permeability vs lab permeability of compacted dolostone thin sections. (b) Modified image permeability vs lab permeability of highly porous dolostone thin sections. (c) Image permeability vs image porosity of all fossiliferous dolostone thin sections.

3.2.2 Petrographical and mineralogical reservoir characterizations using PIA

3.2.2.1 Petrographical reservoir characterization

Figure 7 (a-b) shows compacted micro-crystalline non-clastic texture of dolomite crystals with non-effective and isolated pores, indicating no connectivity and low permeability, while figure 7 (c) shows highly dissolved and leached micro-crystalline non-clastic texture of dolomite crystals with high intraparticle (within the grains) and interparticle (between the grains) pores and vugs, indicating effective connectivity and high permeability. Noting that the rocks are impregnated with blue dye-resin to display porosity and that Dolomite crystals are developed mainly due to the growth of grains that are precipitated small and nourished by a saturated solution in pores, and pressurized by overburden sediments, with fractures encompassing secondary dolomite that indicates that marine environment was once existing.

3.2.2.2 Mineralogical reservoir characterization

Lithology by thin section images observation:

Figure 7 (a) shows that the compacted fossiliferous dolostone sample is made up of many well crystalline dolomite particles (white rhombi), and very few quartz grains (black or grey color), while figure 7 (b) shows that the compacted calcareous dolostone sample is made up

of calcite crystals and well crystalline dolomite particles. Moreover, Figure 7 (c) shows that the highly porous fossiliferous dolostone sample is made up of fossiliferous dolostone crystals (white rhombi).

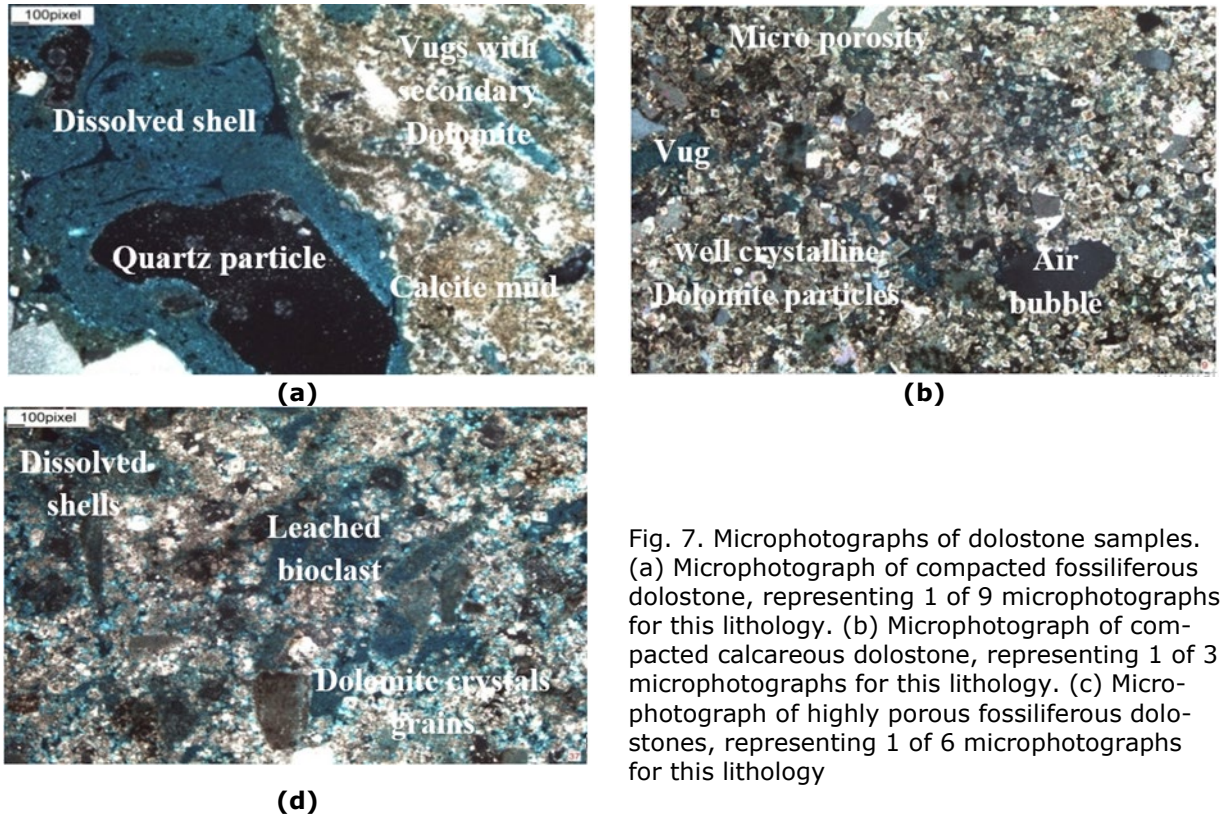

Fig. 7. Microphotographs of dolostone samples. (a) Microphotograph of compacted fossiliferous dolostone, representing 1 of 9 microphotographs for this lithology. (b) Microphotograph of compacted calcareous dolostone, representing 1 of 3 microphotographs for this lithology. (c) Microphotograph of highly porous fossiliferous dolostones, representing 1 of 6 microphotographs for this lithology

Other lithology references:

a) XRD analysis

As indicated in Figure 8, XRD analyses of compacted fossiliferous dolostones, of compacted calcareous dolostones, and highly porous fossiliferous dolostones show that dolomite has the highest XRD peak and so intensity, indicating dolomite lithology and mineral compositions of 96% Dolomite ($CaMg(CO_3)_2$), 3% Quartz (SiO_2), and 1% calcite, magnesian (Mg.064 Ca.936) (C O3), of 85 % dolomite , and 15% calcite, magnesian and of 100% dolomite, respectively. Noting that, the secondly listed samples are named calcareous due to the 15% calcite composition existing.

b) Core Visual Observations

Compacted fossiliferous dolostone samples, compacted calcareous dolostone samples, and highly porous fossiliferous dolostone samples show carbonate core visual observations (yellow and very smooth rock texture (for compacted samples) as well as reddish yellow and rough rock texture (for highly porous samples), with no sand particles intercalated in the cores).

c) Core Plug Densities

Compacted fossiliferous dolostone samples show misleading core plug densities, while compacted calcareous dolostone samples and highly porous fossiliferous dolostone samples show dolomite core plug densities.

- **Lithology Result**

All thin section images observations comply with XRD analyses and core visual observations, regarding the lithology, while core plug densities show misleading results for compacted fossiliferous dolostone samples, which points to the importance of using multiple methods for lithology validation.

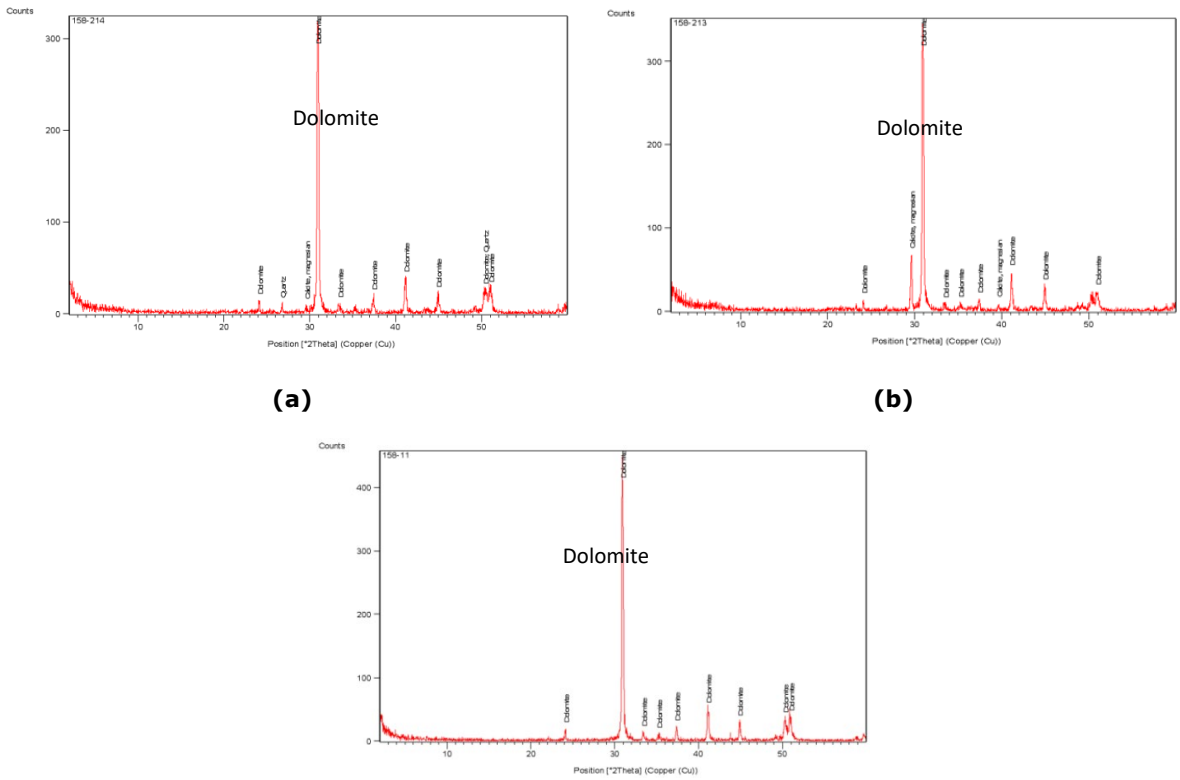

Fig. 8. XRD analysis mineral heights vs position (a) Compacted fossiliferous dolostones XRD mineral heights vs position. (b) Compacted calcareous dolostones XRD mineral heights vs position. (c) highly porous dolostone XRD mineral heights vs position

3.3. Nummulitic limestone samples

3.3.1. Petrophysical reservoir characterization using PIA

After applying the permeability modification as performed in the preceding samples, figure 9 (a-b) along with corresponding multiplying fraction and lowest variance (σ^2), as shown in table 1, indicate that the best permeability equation to be used in Medium Porous Nummulitic Limestones is the Kozeny Carman equation and hydraulic radius approximation with R^2= 0.870 of K image modified Vs K laboratory plot and R^2= 0.808 of K image versus Ø image plot. Noting that, although the proposed equation does not give the highest R^2 values, still it gives R^2 values greater than 0.8, which makes it valid for this lithology, as supported by the lowest variance of the multiplying constant.

3.3.2. Petrographical and Mineralogical Reservoir Characterization Using PIA

Figure 10 shows the micro-crystalline non-clastic texture of limestone crystals taking the form of nummulites. Noting that, the rocks are impregnated with blue dye-resin to display porosity and that the pore space is made up of intraparticle (within the grains) and interparticle (between the grains) pores, reducing grain size, resulting from the dissolution of shells and fossils, and indicating marine environment was once existing with water dissolutions and medium porosity. The pores are both isolated pores, with no connectivity, and effective pores, with connectivity due to the dissolution of water bodies and leaching of limestone crystals, indicating medium porosity and permeability.

Figure 10 shows that the medium porous nummulitic limestone sample is made up of nummulitic limestone crystals (grey color), exhibiting the Nummulites' structure.

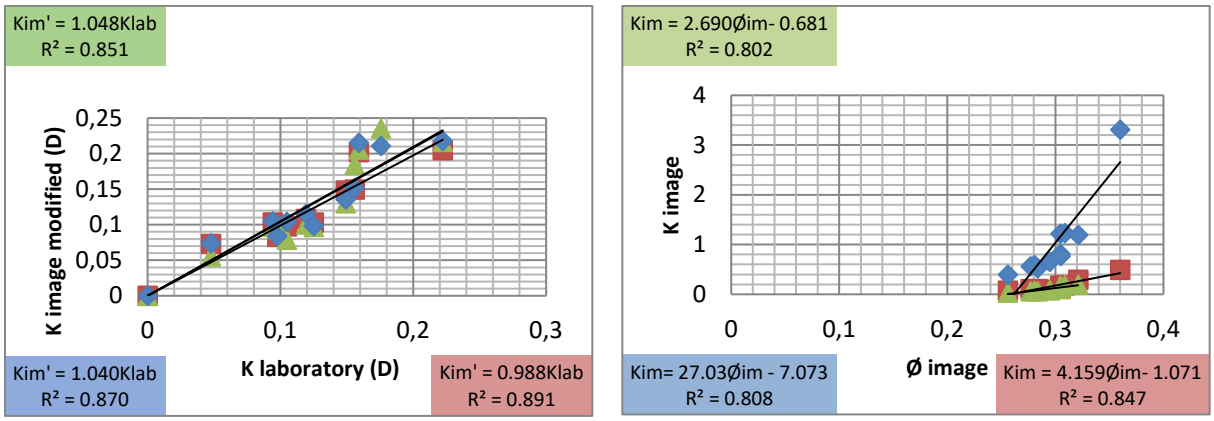

(a) (b)

Fig. 9. Validative plots. (a) Modified image permeability vs lab permeability of medium porous nummulitic limestones. (b) Image permeability vs image porosity of medium porous nummulitic limestones.

3.3.2.1 Mineralogical reservoir characterization

Lithology by thin section images observation:

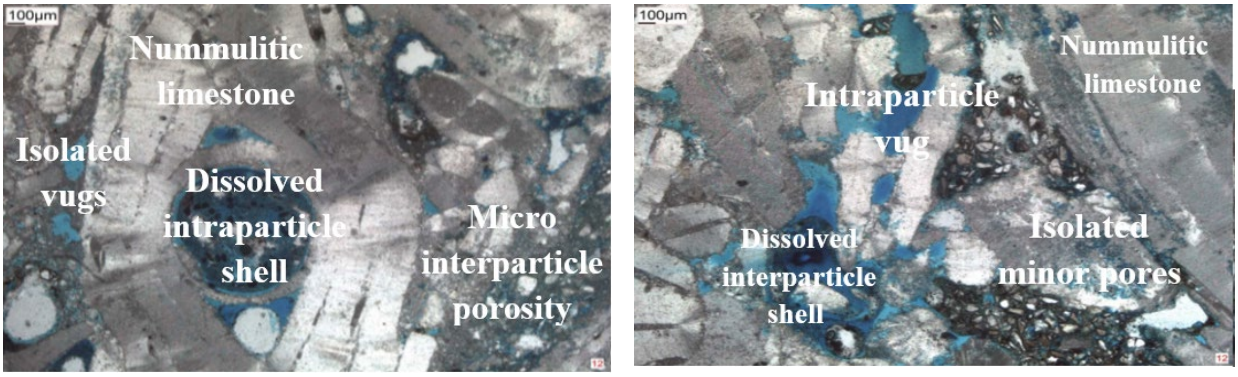

(a) (b)

Fig. 10. Microphotographs of medium porous nummulitic limestones. (a) and (b) represent 2 of the 13 microphotographs for this lithology

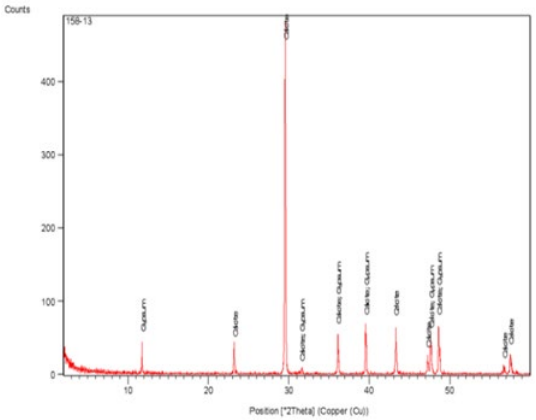

Fig. 11. Nummulitic limestones XRD analysis mineral heights vs position

a) XRD analysis

XRD analysis of medium porous nummulitic limestone shows that calcite has the highest XRD peak and so intensity, indicating limestone lithology and mineral composition of 97% Calcite and 3% Gypsum.

b) Core visual observations

Medium porous nummulitic limestone shows carbonate core visual observations: White and smooth rock texture, with no sand particles intercalated in the cores.

c) Core plug densities

Medium porous nummulitic limestone samples show limestone core plug densities.

Lithology result

Thin section images observations, regarding the lithology, comply with core visual observations, core plug densities, and XRD analysis, which highly validates the lithology observed from thin section images.

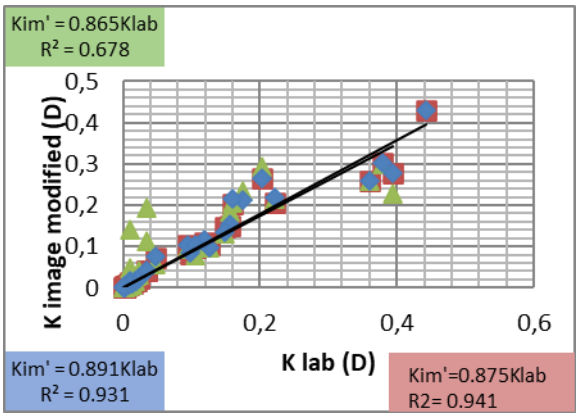

Fig. 12. All samples modified image permeability vs lab permeability

3.4. All the samples

As indicated by high R^2 value and lowest variance (σ^2) of corresponding multiplying fraction of all the samples combined, **t**he best permeability equation for the combined samples is the Kozeny Carman equation and hydraulic radius approximation.

3.4.1. Winland R35 rock typing method and classification for all samples

Figure 13 illustrates the comparison of Winland R35 plots obtained from thin section images and the 3 permeability equations versus that of the laboratory.

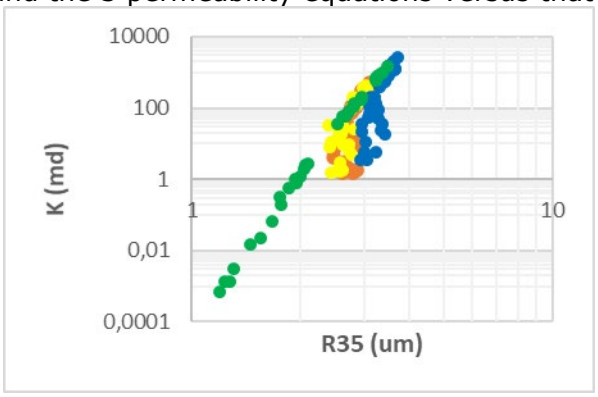

Fig. 13. Winland K versus R_{35} plot

As shown, the laboratory Winland R35 plot (yellow color), which acts as the reference, indicates a single range of throat sizes (um): 2-10, and so macro rock type class [17]. However, not all three other Winland R35 plots obtained from the image match the laboratory rock type class: Both the Kozeny Carman equation and hydraulic radius approximation (blue color), and Kirkpatrick equation and effective medium approximation conductance (red color) match the laboratory, while the Kozeny Carman equation (green color) does not fully match as it indicates two rock classes: meso0.5-2 um throat (sizes) and macro (2-10 um throat sizes) [17]. which again assures that Kozeny Carman equation does not give accurate results and that the other two permeability equations are better.

4. Conclusion

Petrographic image analysis provides a cheap, simple, time-saving, and applicable on small cuttings 2D method to perform petrophysical, petrographical, and mineralogical reservoir characterizations. In this research, reservoir characterization parameters, including porosity and permeability, are estimated using PIA, 2D stained thin section images, and ImageJ software. Also, rock texture and lithology are susccessfully described for all the samples using PIA with the additional privilege of direct eye observation of the microstructure. Three previous permeability equations are modified and applied and permeability correlating factors are established for each lithology. Moreover, Winland R35 rock typing method is applied. Based on the previous experiments and observations, the following conclusions can be drawn:

1) After using most optimum Kozeny constant that equals 5, the Kozeny Carman equation is found to be the least accurate equation, still with accuracies of $R^2 > 0.7$ for most samples'

K image versus K laboratory plots, also approximately half the samples' ratio factors $\frac{\text{Klaboratory}}{\text{KKozeny}}$ show low variances, which is still good and corresponds to nummulitic limestones and highly porous dolostone of average ratio factors of 1.393167 and 0.365367, respectively.

2) The Kozeny Carman equation and hydraulic radius approximation shows good permeability trends, with ratio factors $\frac{\text{Klaboratory}}{\text{KKozenyhydraulic}}$ of average values of 0.186 for dolostones, around 0.3 for sandstones, and 0.182 for nummulitic limestones, and corresponding small variances.
3) After dividing the calculated permeabilities over concluded values of 2 for sandstones, 2.7 for dolostones, 2.8 for pure nummulitic limestone, and 3.6 for gypsum nummulitic limestone, Kirkpatrick equation, and effective medium approximation conductance is found to give good permeability trends, with ratio factors $\frac{\text{Klaboratory}}{\text{Kconductance}}$ of average values of 0.939 for dolostones, of 1.038 for nummulitic limestones, and 0.956 for sandstones, and corresponding small variances.

Noting that, these ratios can be implemented afterward to get the actual laboratory permeability directly from the equation using thin section image parameters, which is a concept validated in figure 12, which uses the three permeability equations after modifications by ratio factors for all the samples. Moreover, results show good accuracy of the coefficient of determination R^2 for porosities and permeabilities of all lithologies, with the conclusion that the Kozeny Carman equation yields the poorest results for all the lithologies, the Kozeny Carman equation and hydraulic radius approximation yields best results for dolostones and nummulitic limestones, and the Kirkpatrick equation and effective medium approximation conductance yields the best results for compacted calcareous sandstones. Also, for all the lithologies combined, the permeability equations are ordered from the most to the least accurate as follow: the Kozeny Carman equation and hydraulic radius approximation, the Kirkpatrick equation and effective medium approximation conductance, then the Kozeny Carman equation, which is a conclusion assured by the K Image modified Vs K Lab Plot, variances (σ^2) of corresponding multiplying fractions, and Winland rock typing and classification method, which shows agreement of all permeability equations' results with those of the laboratory, except the Kozeny Carman equation. Moreover, proper results of mineralogy and petrography are observed, with conclusions and illustrations specific for each lithology, as discussed in earlier sections.

References

[1] Soliman, Ahmed Ashraf, Abdelaziz Nasr El-hoshoudy, and Attia Mahmoud Attia. Assessment of xanthan gum and xanthan-g-silica derivatives as chemical flooding agents and rock wettability modifiers. Oil & Gas Science and Technology, 2020; 75 (12): 1-13.

[2] Mahran S, A Attia, Z Zadeh, and B Saha. Synthesis and characterization of a novel amphoteric terpolymer nanocomposite for enhanced oil recovery applications. ECOS2019 – 32nd International Conference on Efficiency, Cost, Optimisation, Simulation and Environmental Impact on Energy Systems 2019. Wroclaw, Poland: LSBU https://openresearch.lsbu.ac.uk/item/8801v

[3] Moorhouse, W W The Study of Rocks in Thin Section. Harper & Brothers. 1959.

[4] Minagawa, Hideki, Yasuhide Sakamoto, Takeshi Komai, Hideo Narita, Kazutaka Mizutani, Kotaro Ohga, Naoya Takahara, and Tsutomu Yamaguchi. Relation between pore-size distribution and permeability of sediment. The Nineteenth International Offshore and Polar Engineering Conference 2009. Osaka, Japan: ISOPE-I-09-343, OnePetro.

[5] Peng, Sheng, Ahmed Hassan, and Robert G Loucks. Permeability estimation based on thin-section image analysis and 2D flow modeling in grain-dominated carbonates. Marine and Petroleum Geology, 2017; 77: 763-775.

[6] Hossain, Zakir. Relative Permeability Prediction from Image Analysis of Thin Sections. SPE EUROPEC/EAGE Annual Conference and Exhibition 2011. Vienna, Austria: SPE-143606-MS, https://doi.org/10.2118/143606-MS.

[7] Rickman, Douglas, Frank Dale Morgan, Richard M. O'Leary, and David Lesmes. 3-D pore and grain size distributions from 2-D images: Fact or fiction? SEG Technical Program Expanded Abstracts. Society of Exploration Geophysicists, 1990; 849-850.
[8] Tomutsa, L, and A Brinkmeyer. Using image analysis to determine petrophysical properties of reservoir rocks. National Inst. for Petroleum and Energy Research 1990. Bartlesville, OK (USA): NIPER-444.
[9] Jurgawczynski Mathieu. Predicting absolute and relative permeabilities of carbonate rocks using image analysis and effective medium theory. Doctoral dissertation, Imperial College London (University of London) 2007.
[10] Suri, Yatin. Predicting petrophysical properties using SEM Image. SPE Reservoir Characterisation and Simulation Conference and Exhibition 2011. Abu Dhabi, UAE: SPE-144434-MS, https://doi.org/10.2118/144434-MS.
[11] Blair, S C, and J G Berryman. "Estimates of Permeability And Relative Permeability For Sandstone Using Image Analysis of Cross Sections." The 32nd U.S. Symposium on Rock Mechanics (USRMS) 1991. Norman, Oklahoma: ARMA-91-365, OnePetro.
[12] Vocke, C P, H J Deglint, C R Clarkson, C Debuhr, A Ghanizadeh, S Hazell, and M Bustin. Estimation of Petrophysical Properties of Tight Rocks from Drill Cuttings Using Image Analysis: An Integrated Laboratory-Based Approach. SPE Canada Unconventional Resources Conference 2018. Calgary, Alberta, Canada: SPE-189825-MS, https://doi.org/10.2118/189825-MS.
[13] Kameda Ayako, and Jack Dvorkin. Permeability in the thin section. 17th Geophysical Conference ASEG Extended Abstracts 2004. 1-5. https://doi.org/10.1071/ASEG2004ab079
[14] Felipussi, Siovani C, and Waldir L Roque. "Identifying 3D Pores Connectivity from 2D Thin Section Image Analysis." 17th World Petroleum Congress 2002. OnePetro.
[15] Tembely, Moussa, and Ali AlSumaiti. Deep learning for a fast and accurate prediction of complex carbonate rock permeability from 3D micro-CT images. Abu Dhabi International Petroleum Exhibition & Conference 2019. Abu Dhabi, UAE: SPE-197457-MS, https://doi.org/10.2118/197457-MS .
[16] Gunter, G W , D R Spain, E J Viro, J B Thomas, G Potter, and J Williams. Winland pore throat prediction method-a proper retrospect: New examples from carbonates and complex systems. SPWLA 55th Annual Logging Symposium 2014. Abu Dhabi, United Arab Emirates: SPWLA-2014-KKK, OnePetro.
[17] Romero Pedro, Gabriela Bruzual, and Ovidio Suárez. Determination of Rock Quality in Sandstone Core Plug Samples Using NMR. International Symposium of Society of Core Analysts 2002. SCA2002-51.
[18] Al-Qenae, Khaled J, and Salman H Al-Thaqafi. New Approach for the Classification of Rock Typing Using a New Technique for Iso-Pore Throat Lines in Winland's Plot. SPE Annual Caspian Technical Conference & Exhibition 2015. Baku, Azerbaijan: SPE-177327-MS, https://doi.org/10.2118/177327-MS .
[19] Shahat, John S, Mohamed I Balaha, and Mohamed S El-Deab and Attia M Attia. Resistivity zone index: Anew approach in rock typing to enhance reservoir characterization using well log data. Energy Reports, 2021; 7: 711-723.
[20] Mode, AW, OA Anyiam, and EC Anigbogu. The effect of diagenesis on reservoir quality of Mamu Sandstone, Anambra Basin, Nigeria. Journal of the Geological Society of India (Springer), 2016; 87 (5): 583-590.
[21] Pireno, Gadjah E, Emmy Suparka, Dardji Noeradi, and Alit Ascaria. Porosity and Permeability Development of the Deep-Water Late-Oligocene Carbonate Debris Reservoir in the Surroundings of the Paternoster Platform, South Makassar Basin, Indonesia. Journal of Engineering & Technological Sciences, 2015; 47 (6).
[22] Kong, Xiangxin, Zaixing Jiang, Chao Han, Lijing Zheng, Yiming Zhang, Ruifeng Zhang, Jianzhang Tian. Genesis and implications of the composition and sedimentary structure of fine-grained carbonate rocks in the Shulu sag. Journal of Earth Science, 2017; 28 (6): 1047-1063.
[23] Alshibli, Khalid A, Bashar A Alramahi, and Attia Mahmoud Attia. Assessment of spatial distribution of porosity in synthetic quartz cores using microfocus computed tomography (μCT). Particulate science and technology, 2006; 24 (4): 369-380.
[24] Alramahi, Bashar A, Khalid A Alshibli, and Attia M Attia. Influence of Grain Size and Consolidation Pressure on Porosity of Rocks. Site Characterization and Modeling, 2005; 1-13.

[25] Wu, Yaokun, and Siddharth Misra. Quantification of Connectivity in Images. SPE/AAPG/SEG Unconventional Resources Technology Conference 2020. Virtual: URTEC-2020-2937-MS, https://doi.org/10.15530/urtec-2020-2937.
[26] Zhang, Yixin, Rouzbeh Ghanbarnezhad Moghanloo, and Davud Davudov. Pore Structure Characterization of a Shale Sample Using SEM Images. SPE Western Regional Meeting 2019. San Jose, California, USA: SPE-195352-MS, https://doi.org/10.2118/195352-MS
[27] Adams, Anthony E., William Scott MacKenzie, and Cyril Guilford. Atlas of sedimentary rocks under the microscope. Routledge 2017.
[28] Schneider, Caroline A, Wayne S Rasband, and Kevin W. Eliceiri. NIH Image to ImageJ: 25 years of image analysis. Nature methods, 2012; 9 (7): 671-675.
[29] Kohli, Rajiv, and eds. K L Mittal. Developments in Surface Contamination and Cleaning: Applications of Cleaning Techniques: Volume 11, Elsevier, 2018.
[30] Williams, Howel, Francis J Turner, and Charles M Gilbert. Petrology: an introduction to the study of rocks in thin sections. WH Freeman, 1954.

To whom correspondence should be addressed: professor Attia Mahmoud Attia, Faculty of Energy and Environmental Engineering, British University in Egypt (BUE), Elshorouk City, Cairo, Egypt; e-mail: attia.attia@bue.edu.eg